RASĀYAN *J. Chem.*
Vol. 19 | No. 4 | 2299-2306 | October-December | 2026
ISSN: 0974-1496 | e-ISSN: 0976-0083 | CODEN: RJCABP
http://www.rasayanjournal.com
http://www.rasayanjournal.co.in

FACILE SYNTHESIS OF CARBON-MODIFIED CeO_2 NANOCOMPOSITES FOR ADVANCED PHOTOCATALYTIC APPLICATIONS

M. Lallimathi[1], P. Kalisamy[1], M. Suryamathi[2], and M. Venkatachalam[3,✉]
[1]Department of Chemistry, Periyar University, Salem-636 011, Tamil Nadu, India
[2]Department of Chemistry, Govt Arts College (Women), Krishnagiri-635001, Tamil Nadu, India
[3]Department of Chemistry, Govt Arts College (Men), Krishnagiri-635001, Tamil Nadu, India
✉Corresponding author: venkatphd06@gmail.com

ABSTRACT
Carbon-doped cerium oxide (C–CeO_2) nanocomposites were synthesised via a simple co-precipitation method using cerium(III) nitrate and biomass-derived carbon from pomegranate peel. The carbon source was prepared through drying, grinding, and carbonisation, providing an eco-friendly dopant. The nanocomposite was obtained through controlled precipitation followed by calcination. The synthesised nanoparticles were confirmed by using FT-IR Spectroscopy, SEM, EDX Spectroscopy, and powder XRD. Results confirmed the formation of crystalline cubic CeO_2 and the successful incorporation of carbon. Scanning Electron Microscopy analysis revealed the distribution of CeO_2 nanoparticles over a porous carbon matrix. The C–CeO_2 nanocomposite exhibited enhanced physicochemical properties due to synergistic interactions, leading to improved photocatalytic dye degradation. This enhancement is attributed to improved surface area, greater charge separation, and enhanced light absorption. The study demonstrates a simple and sustainable approach for developing efficient materials for wastewater treatment.
Keywords: Carbon-doped CeO_2, Co-Precipitation Synthesis, Biomass-Derived Carbon, Photocatalytic Dye Degradation, Wastewater Treatment.
RASĀYAN *J. Chem.*, Vol. 19, No.4, 2026

INTRODUCTION

Water pollution caused by organic dyes from textile, pharmaceutical, and chemical industries has become a major environmental concern owing to their toxicity, persistence, and resistance to conventional treatment methods.[1–3] Many dyes are non-biodegradable and can generate harmful byproducts, posing serious risks to aquatic ecosystems and human health.[4] Therefore, the development of efficient, sustainable, and cost-effective techniques for wastewater treatment is of great importance. Among various advanced oxidation processes, semiconductor-based photocatalysis has developed as a hopeful approach due to its ability to degrade organic pollutants into harmless end products under light irradiation.[5–7] Because of its superior redox characteristics, large oxygen storage capacity, chemical stability, and non-toxicity, cerium oxide (CeO_2) is a semiconductor material that is extensively researched.[8–10] Oxygen vacancies and the Ce^{3+}/Ce^{2+} redox pair are essential for improving photocatalytic performance.[11] Nevertheless, the efficiency of pure CeO_2 under visible light irradiation is limited by a number of issues, including a large band gap (~3.2 eV) and fast recombination of photogenerated electron–hole pairs.[12, 13] Many modification techniques, including composite creation, metal doping, and non-metal doping, have been investigated to get around these restrictions.[14–16] Among these methods, carbon doping has drawn a lot of interest since it can increase surface area, improve charge separation, and improve light absorption.[17–19] By serving as electron reservoirs, carbon compounds can promote charge transfer and lower recombination losses.[20] Additionally, the incorporation of carbon into CeO_2 can introduce defect states and narrow the band gap, thereby improving visible-light-driven photocatalytic activity.[21,22] Biomass-derived carbon sources are particularly attractive due to their abundance, low cost, and environmental friendliness.[23] In recent years, the utilisation of agricultural waste materials for the synthesis of carbon-based nanomaterials has received considerable attention as part of green chemistry approaches.[24,25] Pomegranate peel, an abundant agricultural byproduct, is rich in carbon content and

http://doi.org/10.31788/RJC.2026.1949933
This work is licensed under a CC BY 4.0 license.

functional groups, making it an excellent precursor for the preparation of activated carbon.[26] The use of such biomass not only reduces waste but also provides a sustainable route for the synthesis of functional nanomaterials.[27] The co-precipitation method is a simple, cost-effective, and accessible method commonly used for synthesizing metal oxide nanoparticles with controlled composition and morphology.[28] This method enables uniform incorporation of dopants and good dispersion of nanoparticles, which are essential for enhanced catalytic performance.[29-30] In this study, carbon-doped cerium oxide (C–CeO_2) nanocomposites were synthesized using a green and facile co-precipitation method, employing pomegranate peel-derived carbon as a sustainable dopant. The produced materials' morphological, structural, and optical characteristics were thoroughly examined. Additionally, the photocatalytic use of the nanoparticles was evaluated for dye degradation when exposed to visible light. Better charge separation, more surface area, and the synergistic interaction between carbon and CeO_2 are all responsible for the higher activity. This study shows how to create effective photocatalysts for wastewater treatment applications in an environmentally responsible manner.

EXPERIMENTAL

Preparation of Carbon Source from Pomegranate Peel

After gathering fresh pomegranate fruits, the skins were removed and carefully cleaned with distilled water to get rid of dust and contaminants. To remove any remaining moisture, the cleaned peels were oven-dried at 80 °C for 12 hours after being air-dried for 24 to 48 hours. To achieve a consistent particle size, the dried peels were ground into a fine powder using a mechanical grinder. After that, the powder was put into a ceramic crucible and carbonized for two to three hours at 400 to 800 °C in a muffle furnace with a restricted air supply. During this process, the organic components decomposed, yielding a carbon-rich material. After carbonisation, the furnace was allowed to cool naturally to room temperature, and the obtained black carbon was collected, finely powdered, and stored in an airtight container for further use as a carbon source or dopant in nanomaterial synthesis.

Synthesis of C-Doped CeO_2 by Co-precipitation Method

C-doped CeO_2 nanoparticles were prepared by a simple co-precipitation method. Cerium(III) nitrate hexahydrate was used as the cerium precursor, and an appropriate carbon source such as glucose (or activated carbon suspension) was employed as the carbon dopant. In a typical synthesis procedure, a calculated amount of $Ce(NO_3)_3 \cdot 6H_2O$ was dissolved in water under constant stirring to obtain a clear homogeneous solution. Separately, the carbon precursor was dispersed in distilled water using ultrasonication for 20–30 mins to ensure uniform distribution. The carbon dispersion was then slowly added to the cerium nitrate solution under vigorous stirring to form a mixed precursor solution. Subsequently, aqueous ammonia solution (NH_4OH) was added dropwise to the above mixture until the pH reached approximately 9–10. In the presence of the carbon source, a pale-yellow precipitate of cerium hydroxide was formed by the slow addition of the precipitating agent. For two to three hours at room temperature, the reaction mixture was continuously agitated to guarantee full precipitation and consistent carbon incorporation into the cerium hydroxide matrix. After that, the precipitate was aged for 12 to 24 hours in order to enhance its crystallinity and promote improved interaction between carbon and cerium species. The precipitate was collected by centrifugation, and purified with water and ethanol to eliminate remaining nitrates and impurities, and then dried in a hot air oven at 80–100 °C for 12 hrs. The dried powder was lastly calcined in a furnace at 400–500 °C for 3–4 hrs in an air atmosphere to convert cerium hydroxide into crystalline CeO_2 and to achieve effective carbon doping within the ceria lattice. The resulting C-doped CeO_2 nanocomposite powder was cooled to room temperature, ground gently, and stored for further characterisation and application studies. The photocatalytic application of Reactive Blue dye (MB) was investigated using C-CeO_2 nanoparticles under ultraviolet (UV) light treatment. A dye solution was prepared by dissolving the dye in 100 mL of distilled water to achieve a 0.01 mM concentration. For the photocatalytic experiment, 100 mL of the dye solution was mixed with 50 mg of the photocatalyst, and the mixture was agitated for half an hour. After that, the mixture was left in the dark to allow the adsorption and desorption processes to balance. Afterwards, the mixture was irradiated with UV light, and the photocatalytic performance was evaluated for every 30 mins. The degradation

efficacy was observed using UV-Vis spectroscopy once the reaction reached equilibrium. The stability of the photocatalyst application was tested by recycling the experiment four times.

RESULTS AND DISCUSSION

The FT-IR spectra of pure carbon and C-doped CeO_2 clearly demonstrate the structural differences and confirm the successful incorporation of cerium oxide into the carbon matrix. A wide absorption band at 3400–3500 cm^{-1} is seen in the spectrum of pure carbon. This band is indicative of hydroxy stretching frequency caused by surface -OH groups and adsorbed moisture. A weak band near 2920–2850 cm^{-1} is attributed to aliphatic C–H stretching vibrations. The prominent band around 1600–1650 cm^{-1} is assigned to C=C stretching of aromatic or graphitic carbon structures, confirming the presence of a conjugated carbon framework. Additionally, minor bands in the 1000–1200 cm^{-1} region are associated with C–O stretching vibrations from oxygen-containing surface functionalities. Importantly, no strong absorption band is observed below 700 cm^{-1}, indicating the absence of metal–oxygen bonds in pure carbon. In contrast, the FT-IR spectrum of C-doped CeO_2 shows significant changes. A strong and distinctive absorption band emerges in the 500–600 cm^{-1} region, while the broad O–H stretching band at about 3400 cm^{-1} and the C=C band near 1600 cm^{-1} remain, indicating the coexistence of carbon in the composite. This band is attributed to Ce–O stretching vibrations and provides clear evidence for the formation of cerium oxide nanoparticles. The bands observed in the 1000–1200 cm^{-1} region may also include contributions from Ce–O–C linkages, suggesting interaction between cerium oxide and carbon surface functional groups. Small shifts in peak positions compared to pure carbon further indicate strong interfacial interaction between CeO_2 and the carbon matrix. Overall, the comparative FT-IR analysis confirms the presence of graphitic carbon, surface oxygen functionalities, and the successful formation and incorporation of CeO_2 within the carbon framework, validating the preparation of the C-doped CeO_2 nanocomposite (Fig.-1).

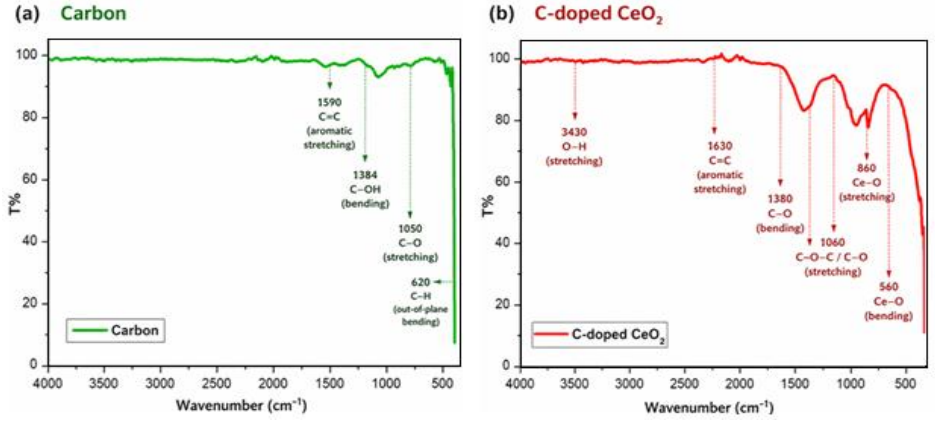


Fig.-1: FT-IR Spectrum of Carbon and C-doped CeO_2

Surface Morphology

The SEM images clearly illustrate the morphological differences between pure carbon and the C-doped CeO_2 nanocomposite. In the Carbon, the material exhibits an irregular, porous, and loosely packed structure. The red dotted circles highlight voids and cavities within the carbon matrix, indicating a highly porous and amorphous nature. Such a structure is typical of biomass-derived carbon and suggests a large surface area with interconnected pores. However, no distinct crystalline particles are visible, confirming that the carbon is predominantly amorphous. In contrast, the C-doped CeO_2 shows a significant change in morphology after the incorporation of cerium oxide. The surface appears more compact and granular, with the formation of aggregated nanostructures. The bright, clustered regions correspond to CeO_2 nanoparticles distributed over the carbon framework. These nanoparticles appear nearly spherical and densely packed, indicating successful nucleation and growth of CeO_2 on the carbon surface. The reduction in visible pores and the formation of nanoparticle clusters suggest that CeO_2 has partially occupied or coated the porous carbon matrix. This confirms strong interaction between carbon and cerium oxide, leading to the formation of a well-integrated nanocomposite. Overall, the SEM analysis

demonstrates that pure carbon possesses a porous, amorphous morphology, whereas the C-doped CeO_2 nanocomposite exhibits a more structured, particle-decorated surface. This structural transformation is crucial for enhancing photocatalytic performance, as it provides more active sites and increases charge transfer efficiency. EDX analysis confirms the presence of Ce, O, and C, indicating successful carbon doping and formation of the C–CeO_2 nanocomposite. SEM image shows a rough, agglomerated surface with uniformly distributed nanoparticles, supporting good interaction between CeO_2 and the carbon matrix (Fig.-2).

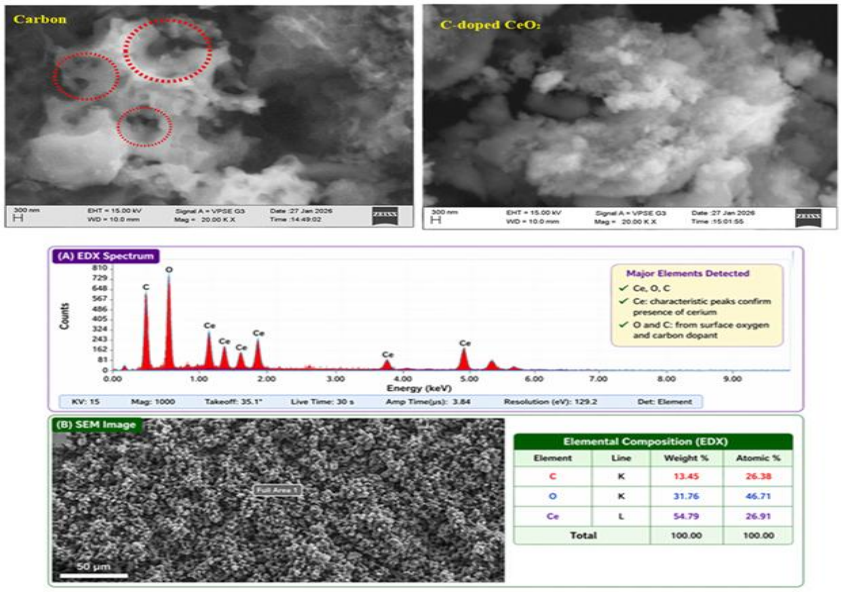


Fig.-2: SEM and EDX Spectrum of Carbon and C-doped CeO_2 Composites

TEM Analysis

The TEM and SAED images (a–d) provide detailed insight into the morphology, particle size, and crystalline nature of the prepared C-doped CeO_2 nanocomposite. In Fig.-3(a), the low-magnification TEM image shows aggregated clusters of particles with irregular and quasi-spherical morphology. The particles appear interconnected, forming chain-like and agglomerated structures. This aggregation is commonly observed in nanomaterials due to high surface energy and indicates the presence of nanoscale particles embedded within the carbon matrix. In Fig.-3(b), the HR-TEM images reveals more clearly defined individual nanoparticles. The particles exhibit nearly spherical shapes with smooth boundaries, and their sizes are in the nanometer range (typically below 50 nm). The contrast difference suggests the coexistence of lighter carbon regions and darker CeO_2 nanoparticles, confirming successful incorporation of cerium oxide into the carbon framework. In Fig.-3(c), a dense accumulation of fine nanoparticles is observed over a larger structure, indicating that CeO_2 nanoparticles are well dispersed and anchored onto the carbon surface. The distribution appears relatively uniform, which is beneficial for catalytic applications as it increases the number of active sites. In Fig.-3(d), the Selected Area Electron Diffraction (SAED) pattern displays distinct concentric rings, confirming the polycrystalline nature of the material. The indexed diffraction rings correspond to the (111), (200), (220), (311), (222), and (400) planes, which are characteristic of the cubic fluorite arrangement of CeO_2. The measured d-spacing values closely match standard JCPDS data, confirming phase purity and good crystallinity of the synthesised nanoparticles. Overall, the TEM and SAED analyses confirm that the C-doped CeO_2 nanocomposite consists of well-dispersed, nanosized, crystalline CeO_2 particles embedded within a carbon matrix. This structural configuration enhances surface area, facilitates charge transfer, and plays a vital role in improving photocatalytic performance.

The powder XRD patterns of pure carbon and C–CeO_2 nanocomposite provide clear evidence for the structural transformation after incorporation of cerium oxide. In the XRD pattern of pure carbon, a broad and low-intensity diffraction peak is observed, typically centred around $2\theta \approx 20–25°$, which corresponds

to the (002) plane of graphitic carbon. This peak's broad shape suggests that the carbon material is primarily amorphous or weakly crystalline, with graphene layers stacked in an unorganised manner. The pure carbon sample's lack of long-range crystalline organization is confirmed by the absence of distinct diffraction peaks. In contrast, the XRD pattern of the C–CeO_2 nanocomposite exhibits distinct and sharper diffraction peaks, confirming the formation of crystalline cerium oxide. The distinctive diffraction peaks of cubic fluorite-structured CeO_2 emerge at around 2θ = 28.5°, 33°, 47°, 56°, 59°, and 69° to the (111), (200), (220), (311), (222), and (400) planes.

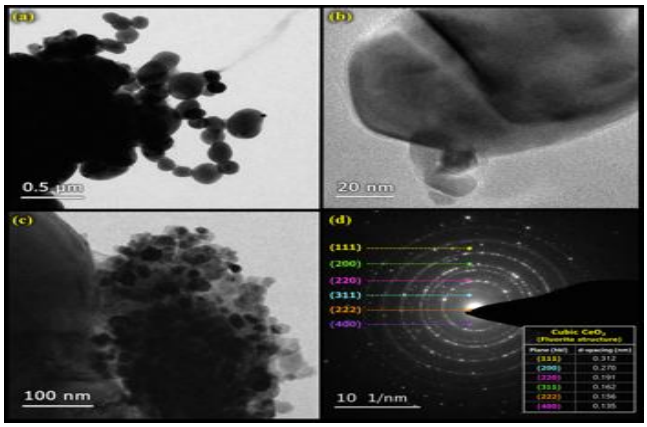


Fig.-3: TEM Analyses of C-doped CeO_2 Composites

These peaks match well with standard JCPDS data for CeO_2, confirming its crystalline phase. The increased peak intensity and sharpness indicate good crystallinity of the CeO_2 nanoparticles. Additionally, the broad carbon peak may still be present but with reduced intensity due to the dominant diffraction signals of CeO_2. Slight peak broadening in the nanoparticle pattern suggests that the CeO_2 particles are in the nanometer range. The absence of extra impurity peaks indicates that the synthesised composite is phase pure. Overall, the powder XRD analysis confirms that pure carbon is largely amorphous, whereas the C–CeO_2 composite contains highly crystalline cubic CeO_2 nanoparticles well incorporated within the carbon matrix, demonstrating successful composite formation (Fig.-4).

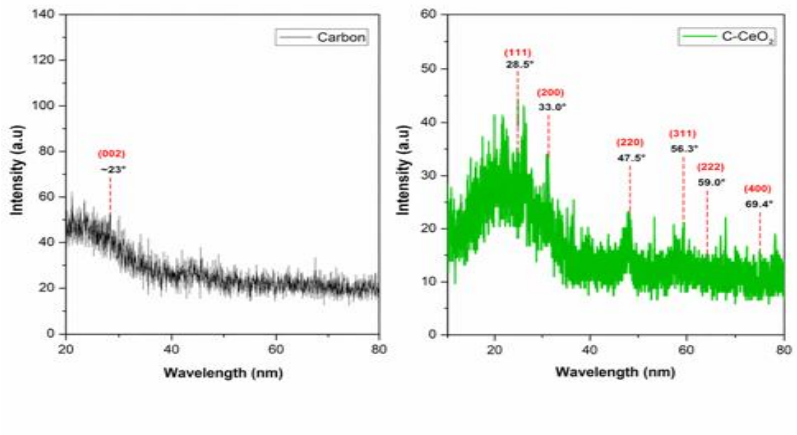


Fig.-4: XRD Spectrum of Carbon and C-doped CeO_2

Photocatalyst Application

The photocatalytic activity of the synthesised C-doped CeO_2 nanocomposite was assessed through the degradation of dye under uv-vis irradiation, and the results are shown in Fig.-(5a–c). The UV–Vis absorption spectra (Fig.-5a) show a gradual decrease in intensity with increasing irradiation time from 0 to 80 minutes, indicating the continuous degradation of the dye molecules. The significant reduction in absorbance confirms the effective photocatalytic activity of the C–CeO_2 nanocomposite. The degradation efficiency is further illustrated in Fig.-5(b), where the normalised concentration (C/C_0) decreases steadily

with irradiation time. Initially, the dye concentration is high ($C/C_0 \approx 1$), but it drops significantly over time, reaching a very low value at 80 minutes, demonstrating efficient removal of the dye from the solution.

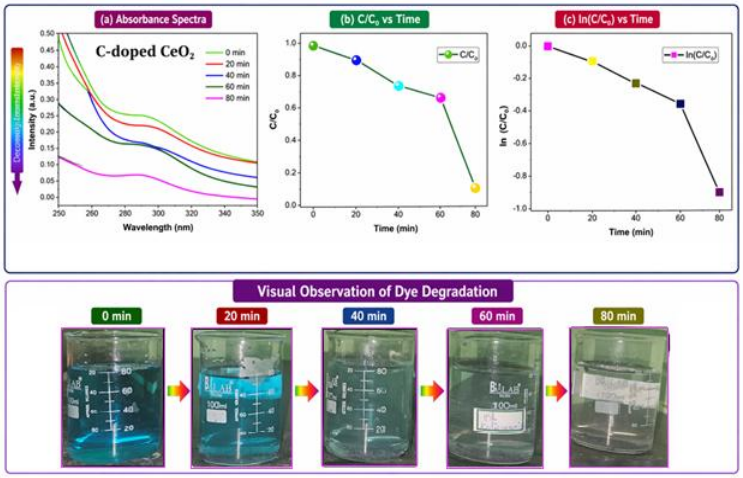


Fig.-5: Photocatalytic Application of Co_3O_4/ZnO/Fe_2O_3 Nano Composite

This trend indicates that the photocatalyst exhibits strong activity and rapid degradation kinetics under light exposure. Furthermore, the kinetic study shown in Fig.-5(c) confirms that the degradation process follows pseudo-first-order kinetics by showing a linear connection between $\ln(C/C_0)$ and time. The slope of the linear plot corresponds to the apparent rate constant, indicating a relatively fast reaction rate. Overall, the enhanced photocatalytic performance of C-doped CeO_2 can be attributed to carbon doping, which improves light absorption and promotes efficient separation of photogenerated electron–hole pairs. This lowers recombination losses and promotes the production of reactive species that are essential to the breakdown of dye compounds, such as hydroxyl (•OH) and superoxide radicals ($\bullet O_2^-$). The results clearly demonstrate that the synthesised nanoparticles are a highly effective photocatalysts for wastewater treatment applications.

CONCLUSION

In this study, carbon-doped CeO_2 nanocomposites were successfully synthesised via a simple co-precipitation method using biomass-derived carbon as a sustainable dopant. The characterisation results (FT-IR, SEM, EDX, TEM, and XRD) confirmed the formation of crystalline cubic CeO_2 and its effective incorporation within the carbon matrix, resulting in improved structural and morphological properties. The nanocomposite exhibited enhanced surface area, better dispersion of nanoparticles, and strong interfacial interaction between carbon and cerium oxide. Due to improved charge separation, decreased electron-hole recombination, and increased light absorption as a result of carbon doping, photocatalytic investigations showed notable dye degradation efficiency under light irradiation, following pseudo-first-order kinetics. Overall, the developed C–CeO_2 nanocomposite presents a cost-effective, eco-friendly, and efficient photocatalyst, showing great potential for environmental remediation and photocatalytic applications.

ACKNOWLEDGMENTS

We would like to express our sincere appreciation to GV Research Organisation in India, Tamil Nadu, Salem-636011 (Reg. No: TN-20-0123282) for their support and contribution to this research.

CONFLICT OF INTERESTS

The authors declare that there is no conflict of interest.

AUTHOR CONTRIBUTIONS

The present work is related to *SDG-7: Affordable and Clean Energy*. All the authors contributed significantly to this manuscript, participated in reviewing/editing and approved the final draft for publication. The research profile of the authors can be verified from their ORCID ids, given below:

M. Lallimathi http://orchid.org/0000-0002-5427-5144
P. Kalisamy http://orchid.org/0009-0001-3104-0959
M. Suryamathi http://orchid.org/0000-0001-5368-8388
M. Venkatachalam http://orchid.org/0000-0001-8408-9433

Open Access: This article is distributed under the terms of the Creative Commons Attribution 4.0 International License (http://creativecommons.org/licenses/by/4.0/), which permits unrestricted use, distribution, and reproduction in any medium, provided you give appropriate credit to the original author(s) and the source, provide a link to the Creative Commons license, and indicate if changes were made.
Cite this article as: M. Lallimathi *et al.*, *Rasayan J. Chem.*, 19(4), 2299-2306(2026), https://doi.org/10.31788/RJC.2026.1949933

REFERENCES

1. S. Dutta, S. Adhikary, S. Bhattacharya, D. Roy, S. Chatterjee, A. Chakraborty, D. Banerjee, A. Ganguly, S. Nanda and P. Rajak, *Journal of Environmental Management,* **353**, 120103(2024), https://doi.org/10.1016/j.jenvman.2024.120103.
2. T. Robinson, G. McMullan, R. Marchant, and P. Nigam, *Bioresource Technology*, **77**, 247(2001), https://doi.org/10.1016/S0960-8524(00)00080-8.
3. M. Kumar, A. Mishra, S. K. Patel, J. Kushwaha, S. Singh, V. Mishra, D. Singh, V. Singh, B. S. Giri, R. R. Singhania and D. Singh, *Bioengineering,* **12(10)**, 1043(2025), https://doi.org/10.3390/bioengineering12101043.
4. H. Zollinger, *Color Chemistry: Syntheses, Properties and Applications of Organic Dyes and Pigments*, Wiley-VCH, Weinheim (2003).
5. A. Fujishima, and K. Honda, *Nature*, **238**, 37(1972), https://doi.org/10.1038/238037a0.
6. A. I. Merchant, A. H. Vakili, A. Kocaman and S. S. Abu Amr, *Desalination and Water Treatment,* **319**, 100565(2024), https://doi.org/10.1016/j.dwt.2024.100565.
7. S. B. Beil, S. Bonnet, C. Casadevall, R. J. Detz, F. Eisenreich, S. D. Glover, C. Kerzig, L. Næsborg, S. Pullen, G. Storch, N. Wei and C. Zeymer, *JACS Au*, **4(8)**, 2746(2024), https://doi.org/10.1021/jacsau.4c00527.
8. A. Trovarelli, *Catalysis Reviews*, **38**, 439(1996), https://doi.org/10.1080/01614949608006464.
9. C. Sun, H. Li, and L. Chen, *Energy and Environmental Science,* **5**, 8475(2012), https://doi.org/10.1039/C2EE22282D.
10. M. Nolan, *Journal of Materials Chemistry,* **21**, 9160(2011), https://doi.org/10.1039/C0JM04561K.
11. D. R. Mullins, *Surface Science Reports,* **70**, 42(2015), https://doi.org/10.1016/j.surfrep.2014.12.001.
12. A. E. Herzog, T. J. Michael, A. D. Dunkelberger, M. D. Johannes, D. R. Rolison, P. A. DeSario and T. G. Novak, *Nanoscale,* **16(20)**, 9659(2024), https://doi.org/10.1039/D4NR00676C.
13. S. N. Matussin, F. Khan, M. H. Harunsani, Y. M. Kim and M. M. Khan, *ACS Omega,* **8(13)**, 11868(2023), https://doi.org/10.1021/acsomega.2c07058.
14. H. Xu, S. Ouyang, P. Li, T. Kako, and J. Ye, *Journal of Physical Chemistry C,* **114**, 17978(2010), https://doi.org/10.1021/jp1059223.
15. S. Bashir, A. Jamil, A. Alazmi, M. S. Khan, I. A. Alsafari and M. Shahid, *Optical Materials*, **135**, 113264(2023), https://doi.org/10.1016/j.optmat.2022.113264.
16. X. Chen, and S. S. Mao, *Chemical Reviews,* **107**, 2891(2007), https://doi.org/10.1021/cr0500535.
17. C. C. Wang, X. H. Yi, and P. Wang, *Applied Catalysis B: Environmental,* **247**, 24(2019), https://doi.org/10.1016/j.apcatb.2019.01.016.
18. Y. Zhang, X. Liu, H. Wang, J. Li, Z. Chen, L. Wang and Y. Zhao, *ACS Applied Materials & Interfaces,* **13(29)**, 3464(2021), https://doi.org/10.1021/acsami.1c01879.
19. F. Bu, R. Yuan, Z. Zhang, J. Wang, J. Liu and Y. C. Yong, *Inorganic Chemistry Frontiers,* **12(2)**, 801(2025), https://doi.org/10.1039/D4QI02386B.
20. P. V. Kamat, *Journal of Physical Chemistry C,* **111**, 2834(2007), https://doi.org/10.1021/jp066952u.
21. H. Li, J. Shang, Z. Ai, and L. Zhang, *Environmental Science and Technology,* **52**, 8659(2018), https://doi.org/10.1021/acs.est.8b01999.

22. Y. Zhang, Z. R. Tang, X. Fu, and Y. J. Xu, *ACS Nano*, **4**, 7303(2010), https://doi.org/10.1021/nn1024219.
23. O. Ioannidou, and A. Zabaniotou, *Renewable and Sustainable Energy Reviews,* **11**, 1966(2007), https://doi.org/10.1016/j.rser.2005.12.002.
24. E. Almaraz-Vega, A. I. Morales-Vargas, G. Gómez Delgado, L. Castellanos-Arteaga, O. Iñiguez Gómez and C. C. Flores Salcedo, *Nanomaterials,* **16(1)**, 75(2026), https://doi.org/10.3390/nano16010075.
25. D. Mohan, and C. U. Pittman, *Journal of Hazardous Materials,* **137**, 762(2006), https://doi.org/10.1016/j.jhazmat.2006.06.060.
26. K. Y. Foo, and B. H. Hameed, *Chemical Engineering Journal,* **180**, 66(2012), https://doi.org/10.1016/j.cej.2011.11.007.
27. A. Jain, R. Balasubramanian, and M. P. Srinivasan, *Chemical Engineering Journal,* **283**, 789(2016), https://doi.org/10.1016/j.cej.2015.08.051.
28. K. Byrappa, and T. Adschiri, *Progress in Crystal Growth and Characterization of Materials,* **53**, 117(2007), https://doi.org/10.1016/j.pcrysgrow.2007.04.001.
29. P. P. Dagwar, N. Ramadan, S. S. Iqbal, J. Singh, L. K. Moganti, D. M. Abdo and D. Dutta, *Environmental Science: Advances*, **5**(5), 1213(2026), https://doi.org/10.1039/D6VA00002A.
30. Z. L. Wang, *Journal of Physics: Condensed Matter,* **16**, R829(2004), https://doi.org/10.1088/0953-8984/16/25/R01.

[RJC-9933/2026]